# The role of the boundary conditions in the Wigner-Seitz approximation applied to the neutron star inner crust.

M. Baldo[a], E.E. Saperstein[b] and S.V. Tolokonnikov[b]

[a]INFN, Sezione di Catania, 64 Via S.-Sofia, I-95123 Catania, Italy
[b] Kurchatov Institute, 123182, Moscow, Russia

**Abstract**

The influence of the boundary conditions used in the Wigner-Seitz approximation applied to the neutron star inner crust is examined. The generalized energy functional method which includes neutron and proton pairing correlations is used. Predictions of two versions of the boundary conditions are compared with each other. The uncertainties in the equilibrium configuration $(Z, R_c)$ of the crust, where $Z$ is the proton charge and $R_c$ the radius of the Wigner-Seitz cell, correspond to variation of $Z$ by 2 – 6 units and of $R_c$, by 1 – 2 fm. The effect of the boundary conditions is enhanced at increasing density. These uncertainties are smaller than the variation of $Z$ and $R_c$ coming from the inclusion of pairing. The value of the pairing gap itself, especially at high density, can depend on the boundary condition used.

PACS : 26.60.+c,97.60.Jd,21.65.+f,21.60.-n,21.30.Fe

In the last two decades the interest on the structure of the neutron star inner crust has been stimulated by the increasing number of observational data on the pulsar glitches. The latter are commonly explained in terms of the dynamics of superfluid vortices within the inner crust of neutron stars (see [1] and Refs. therein). By "inner crust" one usually indicates the part of the shell of a neutron star with sub-nuclear densities $0.001\rho_0 \leq \rho \leq 0.5\rho_0$, where $\rho_0$ is the normal nuclear density. According to present-day ideas, the bulk of the inner crust consists mainly of spherically symmetrical nuclear-like clusters which form a crystal matrix immersed in a sea of neutrons and virtually uniform sea of electrons. Such a picture was first justified microscopically in the classical paper by Negele and Vautherin (NV) [2] within the Wigner-Seitz (WS) approximation. Up to now, the WS method remains to be quite popular in this field. Only recently a more consistent band theory was developed for the deep (high density) layers [3], where the "lasagna" or "spaguetti" structure of the crust matter is supposed to be favored, and for

the outer (low density) layers as well [4]. As far as the band theory is quite complicated, the WS method is usually considered as the most practical one for systematic investigation of the inner crust structure in the whole density interval.

NV used for describing the matter of a neutron star crust a version of the energy functional method with density dependent effective mass $m^*(\rho)$. In fact, it is very close to the Hartree-Fock method with effective Skyrme forces. For a fixed average nuclear density $\rho$, the nuclear (plus electron) energy functional is minimized for the spherical WS cell of the radius $R_c$. A cell contains $Z$ protons (and electrons) and $N = A - Z$ neutrons ($A = (4\pi/3)R_c^3\rho$). In addition, the $\beta$-stability condition,

$$\mu_n - (\mu_p + \mu_e) = 0, \tag{1}$$

has to be fulfilled, where $\mu_n$, $\mu_p$ and $\mu_e$ are the chemical potentials of neutrons, protons and electrons, respectively. The minimization procedure is carried out for different values of $Z$ and $R_c$. The equilibrium configuration $(Z, R_c)$ at the considered density corresponds to the absolute minimum in energy among all these possible configurations.

Application of the variational principle to the NV energy functional for a WS cell results in the set of the Shrödinger-type equations for the single particle neutron functions $\phi_\lambda(\mathbf{r}) = R_{nlj}(r)\Phi_{ljm}(\mathbf{n})$, with the standard notation. The radial functions $R_{nlj}(r)$ obey the boundary condition (BC) at the point $r = R_c$. There exist different kinds of the BC. NV used the following one:

$$R_{nlj}(r = R_c) = 0 \tag{2}$$

for odd $l$, and

$$\left(\frac{dR_{nlj}}{dr}\right)_{r=R_c} = 0, \tag{3}$$

for even ones. Let us denote it as BC1. The use of this BC has been partly justified by physical considerations in NV, but the dependence of the results on the BC has never been discussed in detail. It is the purpose of the paper to study this problem at a quantitative level and to establish the corresponding uncertainity, which is inherent to the WS method applied to neutron star crust. For this aim, we compare results obtained for the BC1 with those found for an alternative kind of the BC (BC2) when Eq. (2) is valid for even

$l$ whereas Eq. (3), for odd ones. In principle, two additional kinds of the BC exist when Eq. (2) or Eq. (3) is used for any $l$. As it was noted by NV, these BC have an obvious drawback for the case of the neutron star inner crust as far as they lead to an unphysical irregular behavior of the neutron density $\rho_n(r)$ in vicinity of the point $r = R_c$. Indeed, $\rho_n(r)$ vanishes in this point in the first case and has a maximum in the second one. On the contrary, $\rho_n(r)$ is almost constant nearby the point $r = R_c$ in the case of the BC1 or BC2.

It should be noted that the pairing effects were not taken into account in [2] since it was supposed that they are not important for the structure of the crust. The reason of such an assumption is the rather small contribution of the pairing effects to the total binding energy of the system under consideration. Recently, we have generalized the NV approach to describe the inner crust by explicitly including the neutron and proton pairing correlations [5, 6, 7, 8] in a self-consistent way. It turned out that in the whole interval of $\rho$ the equilibrium configuration $(Z, R_c)$ changes significantly due to pairing.

We used the generalized energy functional method [9] which incorporates the pairing effects into the original Kohn-Sham (KS) [10] method. In this approach, the interaction part of the generalized energy functional (GEF) depends, on equal footing, on the normal densities $\rho_n, \rho_p$, and the abnormal ones, $\nu_n, \nu_p$, as well:

$$E_{int} = \int d\mathbf{r}\mathcal{E}_{int}(\rho(\mathbf{r}), \nu(\mathbf{r})), \tag{4}$$

where $\mathcal{E}_{int}$ is the GEF density. It is the sum of two components, the normal and the anomalous (superfluid) ones:

$$\mathcal{E}_{int} = \mathcal{E}_{norm}(\rho_\tau) + \mathcal{E}_{an}(\rho_\tau, \nu_\tau), \tag{5}$$

where $\tau = n, p$ is the isotopic index. Just as in the KS method, the prescription $m^* = m$ holds to be true.

To describe the central part of a WS cell with the nuclear cluster inside we used the phenomenological nuclear GEF $\mathcal{E}^{ph}$ by Fayans et al. [9] which describes properties of the terrestrial atomic nuclei with high accuracy. For describing neutron matter surrounding the cluster we used a microscopic energy functional $\mathcal{E}^{mi}$ for neutron matter based on the Argonne NN potential $v18$ [11]. The ansatz of [7, 8] for the complete energy functional is a smooth matching of the phenomenological and the microscopic functionals at the cluster surface:

$$\mathcal{E}(\rho_\tau(\mathbf{r}), \nu_\tau(\mathbf{r})) = \mathcal{E}^{ph}(\rho_\tau(\mathbf{r}), \nu_\tau(\mathbf{r}))F_m(r) + \mathcal{E}^{mi}(\rho_\tau(\mathbf{r}), \nu_\tau(\mathbf{r}))(1 - F_m(r)), \tag{6}$$

where the matching function $F_m(r)$ is a two-parameter Fermi function:

$$F_m(r) = (1 + \exp((r - R_m)/d_m))^{-1}. \quad (7)$$

Eq. (6) is applied both to the normal and to the anomalous components of the energy functional. After a detailed analysis, the matching parameters were chosen as follows. The diffuseness parameter was taken to be equal to $d_m$=0.3 fm for any value of the average baryon density of the inner crust and for any configuration $(Z, R_c)$. As to the matching radius $R_m$, it should be chosen anew in any new case, in such a way that the equality

$$\rho_p(R_m) = 0.1\rho_p(0) \quad (8)$$

holds. In this case, on one hand, for $r < R_m$ neutrons and protons coexist inside the nuclear-type cluster, and the use of a realistic phenomenological energy functional seems reasonable. On the other hand, at $r > R_m$ one can neglect the exponentially decaying proton "tails" and consider the system as a pure neutron matter for which an adequate energy functional microscopically calculated can be used. The same matching parameters were used for normal and anomalous parts of (6). As far as practically all the protons are located inside the radius $R_m$, the matching procedure concerns, in fact, only neutrons, protons being described with the pure phenomenological nuclear GEF.

It is worth to mention that for neutron matter region, the ansatz is, in fact, the LDA for the microscopic part of the GEF. As it is commonly known, the LDA works well only provided the density is smoothly varying, whereas it fails in the surface region with a sharp density gradient. The above choice of the matching procedure and the values of the parameters guarantees that this region of a sharp density variation is mainly governed by the phenomenological nuclear part of the GEF which "knows how to deal with it".

For the microscopic part of the normal component of the total energy functional (6) we follow refs. [7, 8] and take the EOS of neutron matter calculated in [12] with the Argonne $v18$ potential on the basis of Brueckner theory, taking into account a small admixture of 3-body force. Its explicit form could be found in the cited articles. The microscopic part of the anomalous component of the GEF in [7, 8] was calculated for the same $v18$ potential within the BCS approximation.

As calculations of [5, 6, 7, 8] have shown, the pairing correlations influence the equilibrium values $(Z, R_c)$ significantly. To explain this effect, it is instructive to analyze the $\beta$-stability condition (1). As far as electrons in the inner crust of a neutron star are ultra-relativistic, the following relation is valid: $\mu_e \simeq (9\pi Z/4)^{1/3}/R_c$. By substituting it into Eq. (1), one finds

$$Z \simeq \frac{4}{9\pi}(\mu_n - \mu_p)^3 R_c^3. \tag{9}$$

The influence of pairing on the chemical potentials $\mu_n$ and $\mu_p$ is much stronger than that on the total binding energy. Their variation may be of the order of the gap value $\Delta \simeq$1–2 MeV. Such a variation of $\mu_n$ or $\mu_p$ may lead to a sizable change of the equilibrium value of $Z$ as far as the difference $(\mu_n - \mu_p)$ is raised to the third power in Eq. (9). The estimate of the change of $Z$ induced by this variation is as follows: $\delta Z{=}3Z\delta(\mu_n - \mu_p)/(\mu_n - \mu_p)$. For average values of $k_{\rm F}$, the difference $\mu_n - \mu_p \simeq 50 \div 70$ MeV, hence $\delta Z$ could reach several units of $Z$. An additional change of the $Z$ value may appear due to a variation of $R_c$.

Besides, as it can be seen in Fig. 1, the binding energy $E_B$ is rather flat function of $Z$ and different local minima $E_B(Z)$ have often close values of $E_B$. Therefore their relative position may change after switching off the pairing since in general the corresponding contribution to $E_B$ is an irregular function of $Z$. Such a situation does often occur within the WS approach, especially for high density values, due to the shell-type effect in the single-particle neutron spectrum. An example is discussed below.

In the calculations of [5, 6, 7, 8] the NV boundary condition, BC1, was used. Here we repeat the analysis for the case of the boundary condition BC2. Results for the binding energy are shown in Fig. 1. Just as in [7, 8] only even values of Z are used. The detailed comparison is made for $k_{\rm F}{=}0.8$ fm$^{-1}$. Although the two curves $E_B(Z)$ are quite different, the positions of local minima for the BC1 and BC2 are close to each other, the distance being equal to 2 or 4 units of Z. What is of primary importance, the relative position of local minima for BC2 is the same as for BC1. In particular, the positions of the absolute minimum almost coincide ($Z{=}52$ for BC1 and $Z{=}54$ for BC2). These observations permit us to simplify calculations for other values of $k_{\rm F}$. In the case of the BC2, we limit ourselves mainly with the analysis of a vicinity of the absolute minimum for the BC1. The neighborhood of other local minima was analyzed only in the case if they have values of $E_B(Z)$ close to that corresponding to the absolute minimum. It turned out that

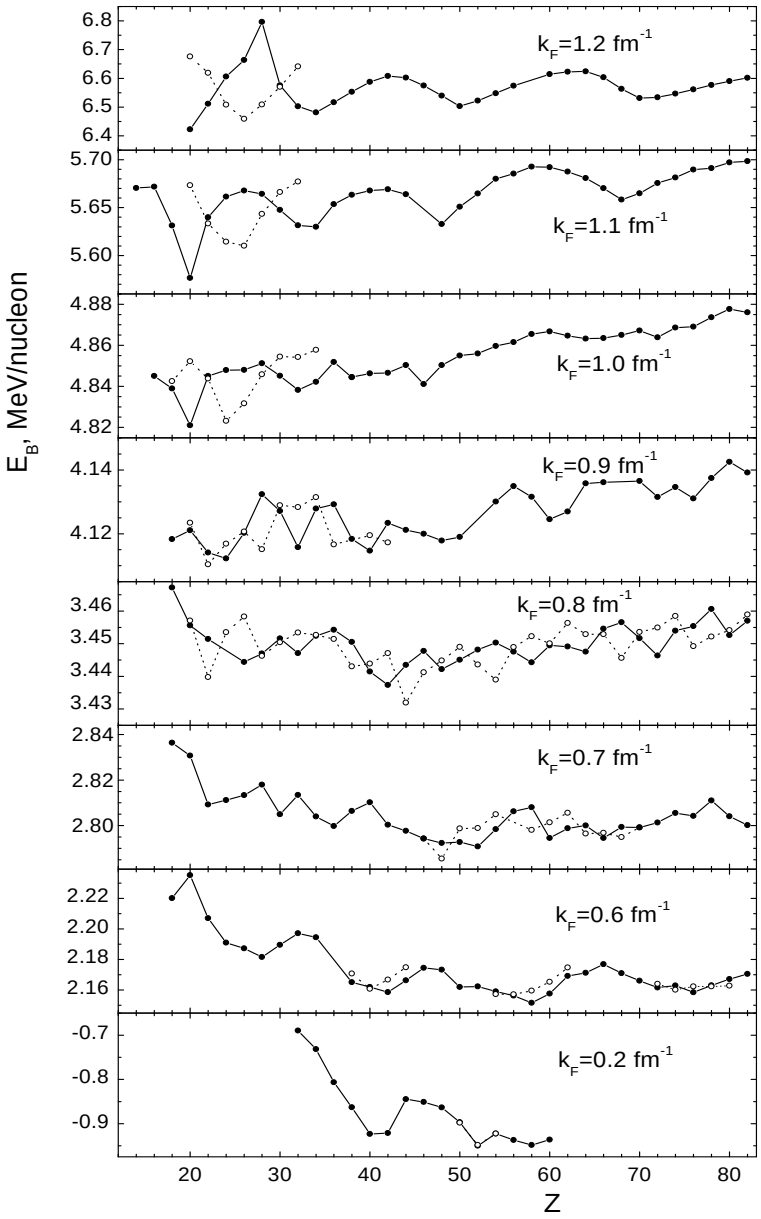


Figure 1: Binding energy per nucleon for various $k_{\rm F}$ in the case of the BC1 (solid circles connected with the solid lines) and the BC2 (open circles connected with the dotted lines).

there is no value of $k_{\rm F}$ for which the relative position of a local minimum and of the absolute one for the BC1 and BC2 is different. In addition to systematic calculations for $k_{\rm F}$=0.6 $\div$ 1.2 fm$^{-1}$, we made an extra one for a small density, $k_{\rm F}$=0.2 fm$^{-1}$, in vicinity of the neutron drip point. In the last case, two curves corresponding to BC1 and BC2 practically coincide. For all other values of $k_{\rm F}$ the absolute minima are shifted by 2, 4 or even 6 units of $Z$.

Table 1: Comparison of properties of equilibrium configurations of the WS cell for two different kinds of the boundary condition

| $k_{\rm F}$ | $Z$ | $R_{\rm c}$, fm | | $E_B$, MeV | | $\mu_{\rm n}$, MeV | | $\Delta_{\rm F}$, MeV | |
|---|---|---|---|---|---|---|---|---|---|
| | | BC1 | BC2 | BC1 | BC2 | BC1 | BC2 | BC1 | BC2 |
| 0.2 | 52 | 57.18 | 57.10 | -0.9501 | -0.9483 | 0.1928 | 0.1942 | 0.04 | 0.05 |
| 0.6 | 58 | 37.51 | 37.48 | 2.1516 | 2.1596 | 3.2074 | 3.2226 | 1.92 | 1.89 |
| | 56 | 36.97 | 36.95 | 2.1563 | 2.1572 | 3.2173 | 3.2193 | 1.91 | 1.89 |
| 0.7 | 52 | 32.02 | 32.04 | 2.7908 | 2.7989 | 3.9876 | 4.0107 | 2.30 | 2.25 |
| | 48 | 31.16 | 31.14 | 2.7924 | 2.7856 | 4.0069 | 3.9873 | 2.29 | 2.32 |
| 0.8 | 42 | 26.90 | 26.91 | 3.4373 | 3.4471 | 4.8454 | 4.8561 | 2.56 | 2.45 |
| | 44 | 27.29 | 27.30 | 3.4435 | 3.4319 | 4.8553 | 4.8198 | 2.53 | 2.56 |
| 0.9 | 24 | 20.26 | 20.30 | 4.1123 | 4.1169 | 5.7340 | 5.7986 | 2.64 | 2.51 |
| | 22 | 19.87 | 19.70 | 4.1141 | 4.1104 | 5.7861 | 5.7170 | 2.62 | 2.54 |
| 1.0 | 20 | 16.69 | 16.90 | 4.8210 | 4.8522 | 6.8525 | 6.7424 | 2.02 | 2.52 |
| | 24 | 18.29 | 18.22 | 4.8479 | 4.8231 | 6.8446 | 6.8920 | 2.52 | 2.29 |
| 1.1 | 20 | 14.99 | 15.33 | 5.5765 | 5.6733 | 7.4288 | 8.0446 | 1.32 | 2.32 |
| | 26 | 16.75 | 17.08 | 5.6677 | 5.6100 | 7.9680 | 8.5398 | 2.28 | 2.02 |
| 1.2 | 20 | 13.68 | 13.95 | 6.4225 | 6.6762 | 8.5814 | 9.1898 | 1.21 | 1.56 |
| | 26 | 15.21 | 14.89 | 6.6639 | 6.4587 | 9.0825 | 9.3413 | 1.25 | 0.86 |

Comparison of different properties of the equilibrium configuration of the WS cell for various values of $k_{\rm F}$ in the case of the BC1 and BC2 is presented in Table 1. There are two lines for every value of $k_{\rm F}$. The first one is given for the $Z$ value corresponding to the minimum of $E_B$ in the case of the BC1, the second one, for the BC2. The only exception is $k_{\rm F}$=0.2 fm$^{-1}$ when these two values of $Z$ coincide. In the last two columns, the average value $\Delta_{\rm F}$ of the diagonal matrix element of the neutron gap at the Fermi surface is given. The averaging procedure involves 10 levels above $\mu_n$ and 10 levels below.

One can see that the influence of the BC is enhanced at increasing values of $k_{\rm F}$. Especially strong variation of $\Delta_{\rm F}$ and $\mu_n$ takes place in the cases of $k_{\rm F}$=1.1 fm$^{-1}$ and $k_{\rm F}$=1.2 fm$^{-1}$ (Fig. 2). To illustrate the influence of the

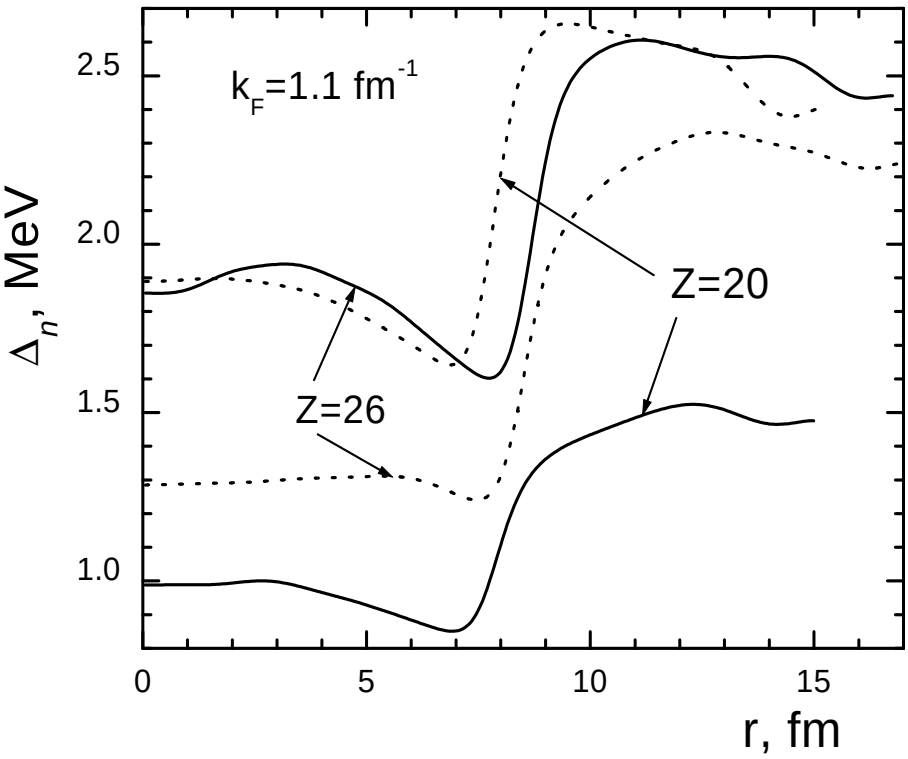


Figure 2: The neutron gap for $k_{\rm F}$=1.1 fm$^{-1}$, $Z$=20 and $Z$=26, in the case of the BC1 (solid lines) and the BC2 (dashed lines).

BC to the neutron gap in the first case, the gap function $\Delta_n(r)$ is drawn for both values of $Z$ and both kinds of the BC. The most strong variation of the gap occurs in the case of $Z$=20. To understand the reason of such strong effect, we draw the neutron single particle spectrum $\varepsilon_\lambda$ for this value of $Z$ in Fig. 3 for the BC1 (the left half of the figure) and the BC2 (the right one). The position of the chemical potential $\mu_n$ is shown with dots. The two spectra are absolutely different. The reason is the shift $\Delta\varepsilon_\lambda$ of each $\lambda$-level going from BC1 to BC2. The value of this shift is approximately equal to a half of the distance between two neighboring levels with the same $(l, j)$, the sign of the shift being opposite for even and odd $l$. The absolute value of

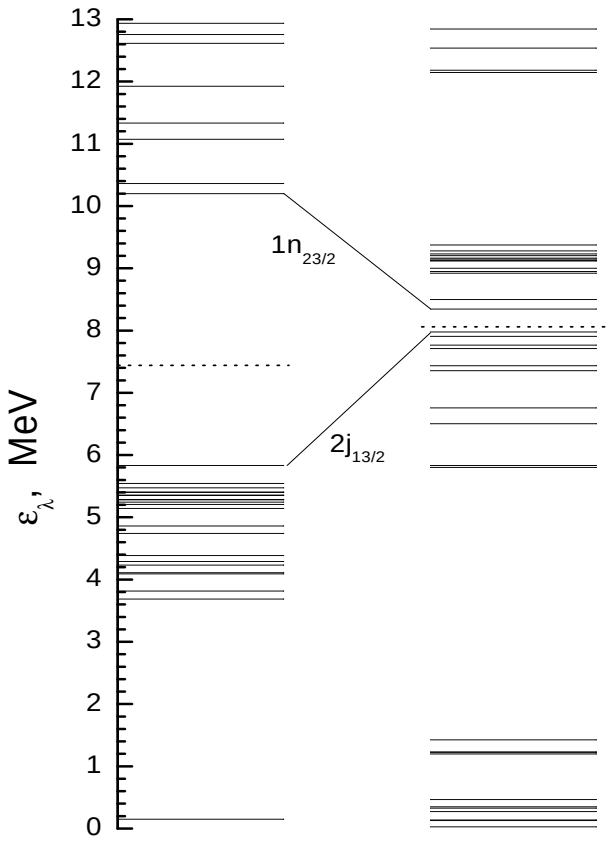


Figure 3: The neutron single-particle spectrum $\varepsilon_\lambda$ for $k_{\rm F}$=1.1 fm$^{-1}$, $Z$=20, in the case of the BC1 (left) and the BC2 (right).

the shift is proportional to $1/R_c^2$ and grows at increasing values of $k_{\rm F}$. The corresponding shifts are shown in Fig. 3 for two states, $2j_{13/2}$ and $1n_{23/2}$, which are the neighbors of $\mu_n$ in the BC1 case. On average, the spectrum is quite dense, however in both cases there is a shell type structure with rather wide intervals between some neighboring levels. If one deals with a big inter-level space in vicinity of $\mu_n$, as in the BC1 case in Fig. 3, one usually obtains a dense set of levels in this region when going to the opposite kind of the BC. In the case of the BC2, big intervals are far from the Fermi surface and do not influence significantly the value of the neutron gap. On the contrary, in the case of the BC1 $\mu_n$ is situated just inside such an interval that suppresses the gap significantly. In principle, the neutron gap could vanish if the interval was wider.

As we see, there are internal uncertainties inherent to the WS method applied to the neutron star inner crust which originate from the kind of the BC used. Only in the case of very small density nearby the neutron drip point predictions of the BC1 and BC2 versions are practically identical. If we deal with $k_{\rm F} \geq 0.6$ fm$^{-1}$, the uncertainty in the equilibrium value of $Z$ is between 2 and 6 units, growing with increase of $k_{\rm F}$. The uncertainty in the value of $R_c$ is, as a rule, about 1 fm and only for $k_{\rm F}$=1.1 fm$^{-1}$ it turns out to be about 2 fm. However, the value of these uncertainties is less than the variation of the equilibrium configuration $(Z, R_c)$ connected with the pairing effects [8]. In the case of high densities, $k_{\rm F} \geq 1$ fm$^{-1}$, the most important uncertainty occurs in the value of the neutron gap $\Delta_n$. It originates from the shell effect in the neutron single-particle spectrum which is rather pronounced in the case of big $k_{\rm F}$ and, correspondingly, small $R_c$ values.

The authors thank N.E. Zein for valuable discussions. This research was partially supported by the Grant NS-1885.2003.2 of The Russian Ministry for Science and Education.

# References

[1] C.J. Pethick, D.G. Ravenhall, Ann. Rev. Nucl. Part. Sci. 45 (1995) 429.

[2] J. Negele, D. Vautherin, Nucl. Phys. A 207 (1973) 298.

[3] B. Carter, N. Chamel, P. Haensel, Nucl. Phys. A 748 (2005) 675.

[4] N. Chamel, arXiv preprint: nucl-th/0512034

[5] M. Baldo, U. Lombardo, E.E. Saperstein, S.V. Tolokonnikov, JETP Lett. 80 (2004) 595.

[6] M. Baldo, E.E. Saperstein, S.T. Tolokonnikov, Nucl. Phys. A 749 (2005) 42.

[7] M. Baldo, U. Lombardo, E.E. Saperstein, S.V. Tolokonnikov, Nuc. Phys. A 750 (2005) 409.

[8] M. Baldo, U. Lombardo, E.E. Saperstein, S.V. Tolokonnikov, Phys. At. Nucl. 68 (2005) 1812.

[9] S.A. Fayans, S.V. Tolokonnikov, E.L. Trykov, D. Zawischa, Nucl. Phys. A 676 (2000) 49.

[10] W. Kohn, L.J. Sham, Phys. Rev. A 140 (1965) 1133.

[11] R.B. Wiringa, V.G.J. Stoks, R. Schiavilla, Phys. Rev. C 51 (1995) 38.

[12] M. Baldo, C. Maieron, P. Schuck, X. Vinas, Nucl. Phys. A 736 (2004) 241.